Cancer Cell
Article

Rapid Decrease in Delivery of Chemotherapy to Tumors after Anti-VEGF Therapy: Implications for Scheduling of Anti-Angiogenic Drugs

Astrid A.M. Van der Veldt,[1,*] Mark Lubberink,[1,6] Idris Bahce,[2] Maudy Walraven,[3] Michiel P. de Boer,[4] Henri N.J.M. Greuter,[1] N. Harry Hendrikse,[1,5] Jonas Eriksson,[1] Albert D. Windhorst,[1] Pieter E. Postmus,[2] Henk M. Verheul,[3] Erik H. Serné,[4] Adriaan A. Lammertsma,[1] and Egbert F. Smit[2]
[1]Department of Nuclear Medicine and PET Research
[2]Department of Pulmonology
[3]Department of Medical Oncology
[4]Department of Internal Medicine
[5]Department of Clinical Pharmacology and Pharmacy
VU University Medical Center, 1007 MB Amsterdam, The Netherlands
[6]PET Centre, Uppsala University Hospital, 751 85 Uppsala, Sweden
*Correspondence: aam.vanderveldt@vumc.nl
DOI 10.1016/j.ccr.2011.11.023

SUMMARY

Current strategies combining anti-angiogenic drugs with chemotherapy provide clinical benefit in cancer patients. It is assumed that anti-angiogenic drugs, such as bevacizumab, transiently normalize abnormal tumor vasculature and contribute to improved delivery of subsequent chemotherapy. To investigate this concept, a study was performed in non-small cell lung cancer (NSCLC) patients using positron emission tomography (PET) and radiolabeled docetaxel ([^{11}C]docetaxel). In NSCLC, bevacizumab reduced both perfusion and net influx rate of [^{11}C]docetaxel within 5 hr. These effects persisted after 4 days. The clinical relevance of these findings is notable, as there was no evidence for a substantial improvement in drug delivery to tumors. These findings highlight the importance of drug scheduling and advocate further studies to optimize scheduling of anti-angiogenic drugs.

INTRODUCTION

Angiogenesis is a critical component for growth and metastatic spread of tumors (Hanahan and Weinberg, 2000; Carmeliet, 2000). Vascular endothelial growth factor (VEGF), which is overexpressed in many human malignancies, is a key regulator of tumor angiogenesis, inducing proliferation, differentiation, and migration of endothelial cells (Ferrara et al., 2003). Consequently, numerous drugs have been developed to target the signaling pathways of VEGF and its receptors (VEGFR; Ferrara and Kerbel, 2005).

Bevacizumab is a humanized monoclonal antibody that targets circulating VEGF and subsequently prevents binding of VEGF to its receptors (Ferrara et al., 2004). Except for metastatic renal cell cancer (Yang et al., 2003), clinical efficacy of single-agent bevacizumab treatment has been very limited in the majority of advanced malignancies (Reese et al., 2001; Cobleigh et al., 2003). Combined with chemotherapy, however, additional value was shown in colorectal (Hurwitz et al., 2004), breast (Miller et al., 2007), and non-small cell lung cancer (NSCLC; Sandler et al., 2006).

In the past years, the normalization theory proposed by Jain (2001) has gained widespread acceptance for explaining additional antitumor effects of inhibitors of VEGF signaling, when combined with cytotoxic drugs. It is hypothesized that anti-angiogenic drugs normalize structurally and functionally abnormal tumor vasculature, thereby reducing interstitial fluid pressure, improving drug penetration, and subsequently

Significance

Optimal scheduling of anti-angiogenic drugs is important for improving efficacy of combination therapy in patients with advanced-stage cancer. In this study, effects of the anti-angiogenic drug bevacizumab on delivery of chemotherapy to non-small cell lung cancer (NSCLC) were investigated using positron emission tomography and ^{11}C-labeled docetaxel. Bevacizumab induced a rapid and significant reduction in delivery of chemotherapy to tumors in NSCLC patients. The study provides a framework for investigating effects of anti-angiogenic drugs on drug delivery to tumors in vivo. In addition, it highlights the importance of drug scheduling and advocates further studies to optimize scheduling of anti-angiogenic drugs.

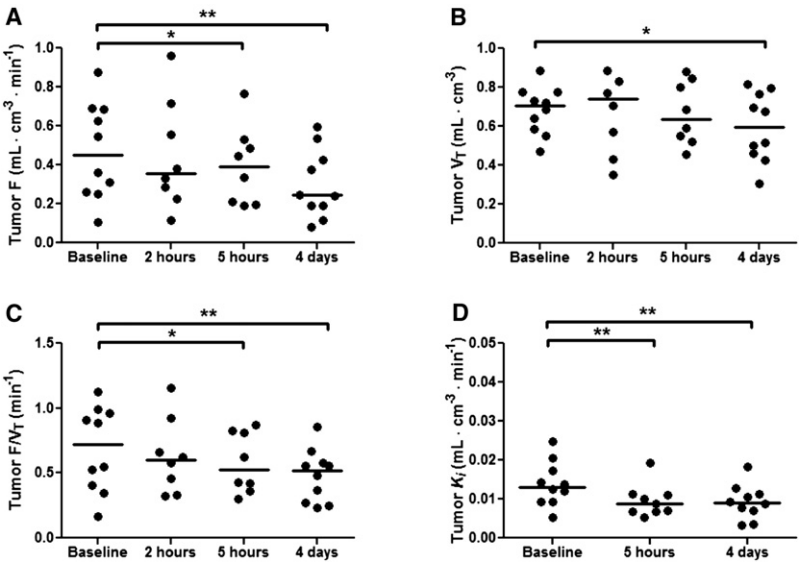

Figure 1. Tumor Measurements in 10 NSCLC Patients at Baseline and after Administration of Bevacizumab

Horizontal bars represent median values.
(A) Perfusion (F).
(B) Volume of distribution of water (V_T).
(C) F/V_T.
(D) Net rate of influx (K_i) of [^{11}C]docetaxel.
*p value < 0.05; **p value < 0.01.

enhancing efficacy of cytotoxic drugs. Exploration of the normalization window may be crucial for optimizing drug scheduling in order to improve clinical efficacy. To date, however, no clinical studies have been reported on the effects of anti-angiogenic agents on drug delivery in cancer patients.

Positron emission tomography (PET) is a noninvasive imaging technique that can be used to monitor drug pharmacokinetics and pharmacodynamics in vivo by radiolabeling drugs of interest with short-lived positron emitting radionuclides (Gambhir, 2002). Previously, the cytotoxic drug docetaxel, a taxane targeting the microtubular network, has been radiolabeled with the radionuclide C-11 ([^{11}C]docetaxel; van Tilburg et al., 2004), enabling in vivo quantification of docetaxel kinetics in lung cancer (Van der Veldt et al., 2011). In the latter study, feasibility of noninvasive PET measurements using radiolabeled water ([^{15}O]H_2O) and [^{11}C]docetaxel was demonstrated and uptake of [^{11}C]docetaxel in lung tumors was found to be associated with tumor perfusion, measured using [^{15}O]H_2O.

The purpose of the present study was to investigate the effects of anti-angiogenic drugs on tumor perfusion and [^{11}C]docetaxel delivery in patients with advanced-stage NSCLC using PET. To this end, bevacizumab was selected, as it is the most selective inhibitor of VEGF signaling among currently approved anti-angiogenic drugs. It was hypothesized that bevacizumab improves drug delivery by normalizing tumor vasculature, which should be reflected by a more homogeneous distribution of perfusion and [^{11}C]docetaxel delivery. A secondary objective of this study was to investigate (systemic) effects of bevacizumab on (1) circulating VEGF levels in plasma; (2) cardiovascular parameters, including blood pressure, cardiac output, and microcirculation in muscle and skin; (3) systemic exposure of [^{11}C]docetaxel; and (4) perfusion and [^{11}C]docetaxel uptake in normal tissues. For the latter, the thyroid gland and the vertebral body were selected. The thyroid gland is known to be highly sensitive to VEGF inhibition (Kamba et al., 2006), whereas the vertebral body may reflect effects of bevacizumab on [^{11}C]docetaxel uptake in bone marrow.

RESULTS

Bevacizumab Induces Rapid Reduction in Tumor Perfusion

To investigate the effect of anti-VEGF therapy on tumor perfusion (F), PET scans using [^{15}O]H_2O, which is a freely diffusible tracer (Hoekstra et al., 2002; Wilson et al., 1992), were performed at baseline and 2 hr, 5 hr, and 4 days after bevacizumab administration. Five hours after bevacizumab administration, there was a significant reduction in tumor perfusion, which persisted until day 4 (Figures 1A and 2A). In three out of eight patients, tumor perfusion already decreased 2 hr after the end of bevacizumab infusion. Accordingly, tumor perfusion showed median percentage changes of 8% (range −39 to +15%; N = 9; p value = 0.889), −20% (range, −39 to −7%; N = 8; p value = 0.012), and −38% (range, −55 to −4%; N = 10; p value = 0.005) at 2 hr, 5 hr, and 4 days after bevacizumab administration, respectively. In addition, the volume of distribution of water (V_T), a measure of the (viable) fraction of tissue that is able to exchange [^{15}O]H_2O, was decreased at 4 days after bevacizumab administration (Figure 1B), with a median percentage change of −7% (range, −52 to +2%; N = 10; p value = 0.022). Individually, eight out of ten patients showed a reduction in volume of distribution of water. Although both perfusion and volume of distribution of water showed an overall decrease, the reduction in perfusion was more severe, as illustrated by a significant decrease in the ratio of tumor perfusion over volume of distribution (F/V_T; (Figure 1C). Collectively, these findings indicate that the decrease in tumor perfusion is not due to a reduction in tumor tissue, which was confirmed by an unchanged tumor volume on subsequent computed tomography (CT) scans.

Bevacizumab Decreases the Net Influx Rate of [^{11}C]docetaxel in Tumors

To determine whether delivery of chemotherapy is affected by bevacizumab, PET scans using [^{11}C]docetaxel were performed at baseline and 5 hr and 4 days after bevacizumab administration. Kinetics of [^{11}C]docetaxel in tumor tissue are irreversible and can be quantified using Patlak graphical analysis, providing the net influx rate constant (K_i) of [^{11}C]docetaxel in tumor tissue (Patlak et al., 1983; Van der Veldt et al., 2011). Prior to bevacizumab infusion, tumors showed a variable K_i of [^{11}C]docetaxel (median K_i, 0.0132 $ml \cdot cm^{-3} \cdot min^{-1}$; range, 0.0054–0.0247 $ml \cdot cm^{-3} \cdot min^{-1}$; N = 10). After administration of bevacizumab, median K_i of [^{11}C]docetaxel significantly decreased (Figures 1D and 2B), resulting in a median percentage

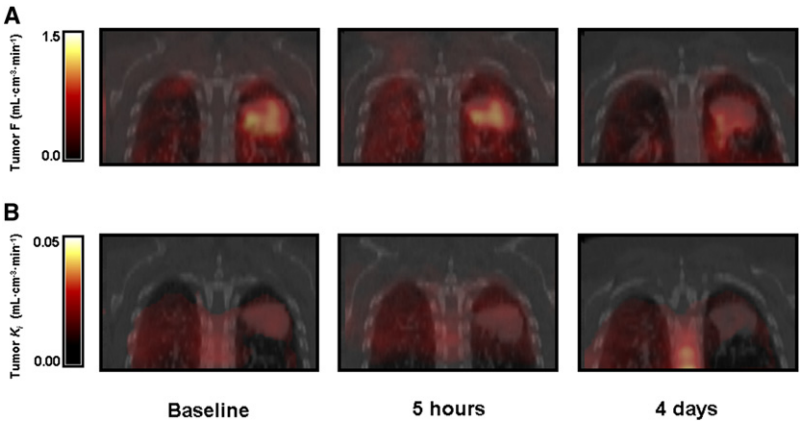

Figure 2. PET-CT Images of a 51-Year-Old Woman with Metastatic Non-Small Cell Lung Cancer

(A) Parametric perfusion images obtained at baseline and at 5 hr and 4 days after bevacizumab administration. In the whole tumor, the mean perfusion changed from 0.875 $ml \cdot cm^{-3} \cdot min^{-1}$ at baseline to 0.765 $ml \cdot cm^{-3} \cdot min^{-1}$ at 5 hr and 0.535 $ml \cdot cm^{-3} \cdot min^{-1}$ at 4 days.

(B) Patlak images of [^{11}C]docetaxel uptake obtained at baseline and at 5 hr and 4 days after bevacizumab administration. In the whole tumor, the mean K_i of [^{11}C]docetaxel changed from 0.0205 $ml \cdot cm^{-3} \cdot min^{-1}$ at baseline to 0.0193 $ml \cdot cm^{-3} \cdot min^{-1}$ at 5 hr and 0.0127 $ml \cdot cm^{-3} \cdot min^{-1}$ at 4 days.

F, perfusion; K_i, net influx rate constant.

change of −22% (range, −51 to −4%; N = 9; p value = 0.008) and −34% (range, −61 to −16%; N = 10; p value = 0.005) at 5 hr and 4 days, respectively. In line with the decrease in the volume of distribution of water, the distribution volume of [^{11}C]docetaxel, which can be obtained from the Patlak plot, also showed a decline on day 4 with a median percentage change of −14% (range, −24 to + 20%; N = 10; p value = 0.052). Before administration of bevacizumab, [^{11}C]docetaxel K_i was associated with tumor perfusion (Spearman's ρ = 0.626; N = 10; p value = 0.053). As two patients had one missing scan (either [^{11}C]docetaxel PET or [^{15}O]H_2O PET), this correlation could not be evaluated at 5 hr. At 4 days, the correlation between [^{11}C]docetaxel K_i and perfusion showed a slight decrease (Spearman's ρ 0.564; N = 10; p value = 0.090).

Tumor Heterogeneity of [^{11}C]docetaxel Uptake Is Not Affected by Bevacizumab

As it is assumed that normalization of tumor vasculature results in a more homogenous distribution of perfusion and drug delivery, spatial distributions of tumor perfusion, volume of distribution of water, and [^{11}C]docetaxel K_i were analyzed on a voxel-by-voxel basis using histogram analysis. For the K_i of [^{11}C]docetaxel, only the median kurtosis of the histograms showed a trend toward an increase from 2.60 at baseline to 3.11 (N = 9; p value = 0.051) and 2.97 (N = 10; p value = 0.059) at 5 hr and 4 days, respectively, whereas standard deviation and kurtosis of the other histograms (F and V_T) did not change. When histogram analysis was applied to separately analyze tumor center and rim, larger tumors showed lower perfusion and lower values of [^{11}C]docetaxel K_i in the center than in the rim. When all primary tumors were analyzed, median baseline values, however, were not significantly different (N = 10; p value = 0.739 and 0.579, respectively). At 5 hr and 4 days after bevacizumab administration, mean, median, minimum, and maximum values of tumor perfusion and [^{11}C]docetaxel K_i showed the same degree of reduction (p value < 0.05) in the whole tumor, as in the center and the rim separately. In addition, the volume of distribution of water showed a significant decrease in both center and rim at 4 days (N = 10; p value < 0.05). Standard deviation and kurtosis of all histograms (F, V_T, and [^{11}C]docetaxel K_i) did not change in the center and the rim, except for a decreased standard deviation of perfusion in the center at 5 hr (N = 8; p value = 0.028). Furthermore, changes in perfusion, volume of distribution of water, and [^{11}C]docetaxel K_i were not associated with baseline tumor volumes. Collectively, these results indicate that bevacizumab induces an overall decrease in perfusion, volume of distribution of water, and [^{11}C]docetaxel K_i in tumors without significantly affecting tumor heterogeneity.

Decrease in [^{11}C]docetaxel Delivery to Tumors Is Accompanied by Rapid Reduction in Circulating VEGF

Plasma levels of circulating VEGF were measured to evaluate whether the rapid decrease in [^{11}C]docetaxel K_i in tumors was supported by a rapid decrease in free VEGF. As VEGF is mainly transported by platelets (Verheul et al., 1997), circulating VEGF was assessed in both platelet-poor and platelet-rich plasma. At 3 hr, administration of bevacizumab resulted in a significant decrease in circulating VEGF in platelet-rich plasma (N = 7; p value = 0.018; Figure 3). In the majority of patients, free VEGF in plasma was completely neutralized within 3 hr and seemed to recover in part after 4 days. Comparable changes in VEGF levels were measured in platelet-poor plasma.

A Reduction in [^{11}C]docetaxel Delivery to Tumors Is Not Associated with Cardiovascular Parameters

Because arterial hypertension and cardiotoxicity are commonly reported side effects associated with inhibitors of VEGF/VEGFR-2 signaling (Chen and Cleck, 2009), it was investigated whether the rapid decrease in tumor perfusion and [^{11}C]docetaxel K_i was accompanied by early onset cardiovascular changes. A single infusion of bevacizumab did not affect systolic and diastolic blood pressure during the first 4 days (Figures 4A and 4B). Median cardiac output as derived from first pass dynamic [^{15}O]H_2O PET scans (Knaapen et al., 2008), however, showed a trend toward a reduction at day 4 (from 6.9 $l \cdot min^{-1}$ to 6.0 $l \cdot min^{-1}$; N = 9; p value = 0.051; Figure 4C). As inhibitors of VEGF/VEGFR-2 signaling may induce so-called rarefaction (Mourad et al., 2008), that is, a reduction in the number of arterioles or capillaries within vascular beds of various tissues (e.g., muscle and skin), muscle perfusion in the erector spinae, as well as capillary density in the skin, were measured. Muscle perfusion was obtained from the [^{15}O]H_2O images, whereas nail-fold capillaries in the dorsal skin of the third finger were examined using a capillary microscope (Serné et al., 2001). Perfusion in the erector spinae muscle and capillary density in the skin did not change during the first 4 days after administration of

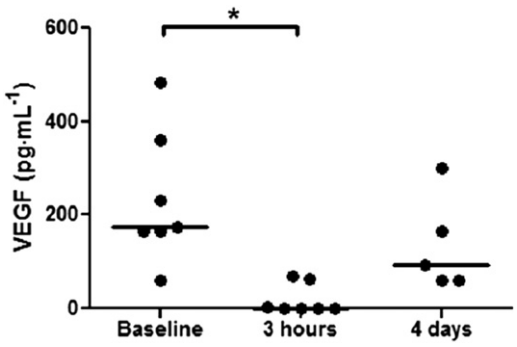

Figure 3. Platelet-rich Plasma Levels of VEGF in Seven Individual Patients at Baseline and after Administration of Bevacizumab

Vascular endothelial growth factor levels were corrected for platelet count and are expressed in pg·ml^{-1} per 200,000 platelets·μl^{-1}. Horizontal bars represent median values.

*p value < 0.05.

bevacizumab (Figures 4D, 4E, and 4F). Of note, [^{11}C]docetaxel K_i in muscle tissue (median K_i, 0.0072 ml·cm^{-3}·min^{-1}; range, 0.0029–0.0104 ml·cm^{-3}·min^{-1}) was lower than that in tumor tissue (N = 10; p value = 0.002). The K_i of [^{11}C]docetaxel in muscle tissue was neither associated with perfusion nor affected by bevacizumab.

Bevacizumab Increases Systemic Exposure of [^{11}C]docetaxel

To investigate whether decreased [^{11}C]docetaxel K_i in tumor tissue was associated with a change in systemic exposure of [^{11}C]docetaxel, plasma clearance of [^{11}C]docetaxel was determined. Four days after bevacizumab administration, plasma clearance of [^{11}C]docetaxel was significantly decreased (N = 10; p value = 0.037), as reflected by a shift to the right of the plasma curves (Figure 5). Consequently, bevacizumab increased the duration of [^{11}C]docetaxel exposure by a reduction in plasma clearance. However, this increased systemic exposure of [^{11}C]docetaxel did not result in increased [^{11}C]docetaxel accumulation in tumor tissue, as the retention index of [^{11}C]docetaxel still decreased after bevacizumab administration (from 0.0155 ml·cm^{-3}·min^{-1} at baseline to 0.0109 ml·cm^{-3}·min^{-1} at day 4; N = 10; p value = 0.005).

Bevacizumab Decreases Thyroid Perfusion

Because normal vessels of the thyroid gland are known for their extensive capillary regression after anti-VEGF therapy (Kamba et al., 2006), thyroid perfusion was also determined using parametric perfusion images. In four out of ten patients, the primary tumor was located in the upper lobes, enabling adequate analysis of thyroid perfusion at baseline and day 4. Four days after bevacizumab administration, median perfusion in the thyroid gland showed a decrease (from 1.316 ml·cm^{-3}·min^{-1} at baseline to 0.585 ml·cm^{-3}·min^{-1} at day 4; p value = 0.068), whereas the volume of distribution of water did not change (p value = 0.273).

[^{11}C]docetaxel Uptake in Bone Marrow Is Not Affected by Bevacizumab

As [^{11}C]docetaxel shows high uptake in bone marrow (Van der Veldt et al., 2010b) and anti-VEGF therapy can block rapid induction of viable circulating endothelial progenitor cells from bone marrow and can inhibit taxane-induced bone marrow colonization in tumors (Shaked et al., 2008), the effects of bevacizumab on [^{11}C]docetaxel uptake in bone marrow was also evaluated. To this end, perfusion and [^{11}C]docetaxel K_i were determined in the vertebral body. Perfusion values were significantly lower in the vertebral body than in tumors (N = 10; p value= 0.003), whereas K_i values of [^{11}C]docetaxel were significantly higher than those in tumors (N = 10; p value < 0.001; Figure 6). In contrast to tumor tissue, there was no association between [^{11}C]docetaxel K_i and perfusion in the vertebral body (Spearman's $\rho = -0.285$; N = 10; p value = 0.425). Perfusion and [^{11}C]docetaxel K_i did not change after bevacizumab administration (Figure 6).

DISCUSSION

Current strategies combining anti-angiogenic therapy with cytotoxic agents have shown proven efficacy in cancer patients, including those with advanced-stage NSCLC (Sandler et al., 2006). Pretreatment with anti-angiogenic drugs may transiently normalize abnormal tumor vasculature (Batchelor et al., 2007) and thereby contribute to improved delivery of subsequent chemotherapy, enhancing efficacy (Jain, 2005). Investigating this process of vasculature normalization in vivo is a major challenge, which is mainly restricted to imaging studies. Whereas conventional imaging studies, such as CT and magnetic resonance imaging, have concentrated on changes in tumor perfusion, the present concept of PET imaging using a radiolabeled drug to study drug delivery in patients after anti-VEGF therapy has not been reported yet. The humanized monoclonal antibody bevacizumab induced an overall decrease in both perfusion and K_i of [^{11}C]docetaxel in tumor tissue within a few hours after bevacizumab administration, a decrease that persisted for at least four days. These findings represent physiological changes in tumors, as measured changes were beyond the known test-retest variability (van der Veldt et al., 2010a and 2011). The large range of changes in perfusion and [^{11}C]docetaxel uptake is most likely due to interpatient differences in tumor response to bevacizumab and partly due to differences in interval between end of bevacizumab infusion and PET scans. Nevertheless, the results indicate a decrease in perfusion and [^{11}C]docetaxel uptake in tumor tissue of all patients. Based on these data, it can be concluded that anti-VEGF therapy is not able to improve drug delivery to tumors but rather has the opposite effect.

Results of the present study are at variance with those obtained by Willett et al. (2004), where improved drug delivery in rectal cancer was postulated partly based on human imaging studies. Tumor perfusion, as determined by dynamic contrast-enhanced CT scanning decreased, whereas the standardized uptake value of 2′-deoxy-2′-[^{18}F]fluoro-D-glucose ([^{18}F]FDG) remained unchanged at 12 days after bevacizumab administration. However, kinetics of [^{18}F]FDG are fundamentally different from those of anticancer drugs, as [^{18}F]FDG reflects glucose metabolism. In the present study, however, the decrease in standard deviation of tumor perfusion in the center of the tumor at 5 hr and the increase in kurtosis of [^{11}C]docetaxel histograms may reflect a more homogenous distribution as

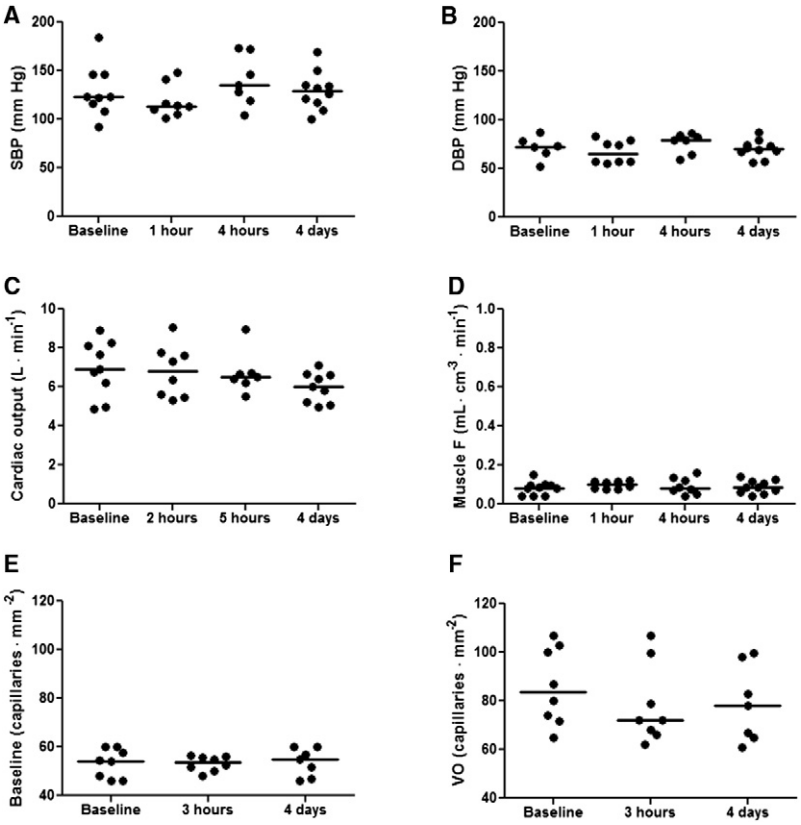

Figure 4. Cardiovascular Variables in Ten NSCLC Patients at Baseline and after Administration of Bevacizumab

Horizontal bars represent median values.
(A) Systolic blood pressure (SBP).
(B) Diastolic blood pressure (DBP).
(C) Cardiac output.
(D) Perfusion (F) in muscle tissue.
(E) Nailfold capillary density.
(F) Nailfold capillary density during venous occlusion (VO).

a result of certain normalization of tumor vasculature. Nevertheless, these possible changes in tumor heterogeneity did not result in improved drug delivery, as bevacizumab infusion caused a rapid and overall reduction in [^{11}C]docetaxel K_i in tumors. In addition, drug uptake may be further impaired by development of tumor necrosis, associated with extensive vascular damage, which usually develops after anti-VEGF therapy. Although it is not possible to define necrotic areas on low-dose CT, development of necrotic areas was possibly reflected by a reduction in the distribution volume of water after 4 days, despite an unchanged total tumor volume on low-dose CT.

Apart from tumor parameters, systemic effects after administration of bevacizumab were evaluated. The rapid changes in tumor perfusion and [^{11}C]docetaxel K_i were associated with an immediate reduction in plasma levels of VEGF, indicating an immediate inhibition of VEGF signaling in the whole body. This rapid neutralization of circulating VEGF also induced a decrease in perfusion of the thyroid gland, whereas perfusion and [^{11}C]docetaxel K_i in the vertebral body and muscle tissue were not affected. In addition, K_i values of [^{11}C]docetaxel in the vertebral body and muscle tissue were essentially different from that in tumor tissue and were not related to perfusion in these normal tissues. These findings imply that tumor tissue shows a difference in sensitivity to VEGF inhibition (Kamba et al., 2006) and in drug delivery as compared with normal tissues. Among the cardiovascular parameters, only cardiac output showed a decrease at day 4, whereas blood pressure and capillary density did not change during the first 4 days after bevacizumab infusion. These findings indicate that the rapid and significant changes in perfusion and [^{11}C]docetaxel K_i in tumors are not caused by immediate development of hypertension, microvascular rarefaction, or a rapid reduction in cardiac output. Consequently, it can be concluded that the decrease in perfusion and [^{11}C]docetaxel K_i in tumors can be attributed to rapid inhibition of VEGF signaling in tumors. As the decrease in perfusion and [^{11}C]docetaxel uptake in tumors is probably too rapid to be solely ascribed to inhibition of tumor angiogenesis, vasoconstrictive effects of anti-angiogenic drugs on tumor vessels, particularly those from the host, should be considered as a potential underlying mechanism. In this regard, inhibition of endothelial nitric oxide synthesis by VEGF inhibitors may be an important factor (Dhaun and Webb, 2010; Syrigos et al., 2011; Ng et al., 2007). Although plasma clearance of [^{11}C]docetaxel decreased slightly after bevacizumab administration, signifying prolonged duration of [^{11}C]docetaxel exposure, this decrease in clearance appeared to be too limited to result in an overall increase in [^{11}C]docetaxel uptake, that is, retention index, by tumors.

Bevacizumab was selected to investigate the effects of anti-angiogenic agents, as it is the most selective inhibitor of VEGF signaling among presently approved anti-angiogenic drugs, and it does not have multiple targets like most tyrosine kinase inhibitors. In addition, the long terminal half-life of 17–21 days (Ferrara et al., 2004) enables sequential measurements after a single administration of bevacizumab. The study was conducted in patients with advanced-stage NSCLC, as noninvasive PET-CT measurements using [^{15}O]H_2O and [^{11}C]docetaxel were previously found to be feasible in this patient group (Van der Veldt et al., 2011). As a result, [^{11}C]docetaxel measurements could be repeated in individual patients who acted as their own control. Although both docetaxel and bevacizumab are active agents for the treatment of advanced lung cancer (Sandler et al., 2006; Kudoh et al., 2006), single-agent bevacizumab is not considered effective for the treatment of NSCLC patients. Consequently, ethically it was not acceptable to prolong the study with PET measurements at later time points. In addition, the localization of the lung tumors did not enable invasive measurements of interstitial fluid pressure (Curti et al., 1993) or sequential biopsies for additional histopathological analyses. Furthermore, use of tracer amounts of docetaxel (microdoses)

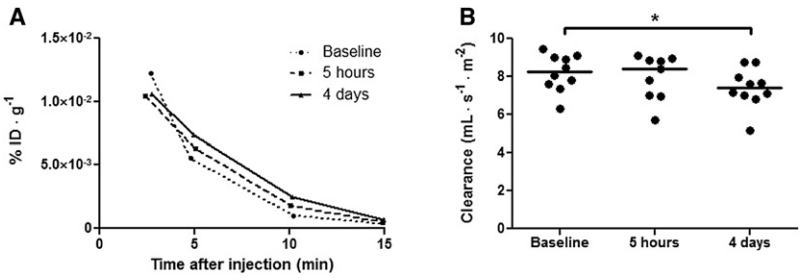

Figure 5. Plasma Clearance of [^{11}C]docetaxel at Baseline and after Administration of Bevacizumab

(A) Example of plasma activity curves of [^{11}C]docetaxel in a patient at baseline and after 5 hr and 4 days following bevacizumab administration. Plasma activity curves are divided by injected dose (ID).

(B) Plasma clearance of [^{11}C]docetaxel in 10 NSCLC patients at baseline and after administration of bevacizumab.

Horizontal bars represent median values.

*p values < 0.05.

may be a potential limitation of the present study, as it is conceivable that the effects of bevacizumab on [^{11}C]docetaxel delivery in tumors may not hold true for pharmacological drug concentrations. However, use of repeated therapeutic doses mixed with the radiolabeled drug, instead of microdoses, will obscure bevacizumab-induced effects, as cytotoxic drugs themselves also affect both tumor perfusion (Dunnwald et al., 2008) and interstitial fluid pressure (Griffon-Etienne et al., 1999) and may modulate the specific targets of the drug under study (Shalli et al., 2005). In a separate study, in which [^{11}C]docetaxel was given at tracer concentrations and during infusion of a therapeutic dose, albeit was possible to predict tumor uptake of (therapeutic) docetaxel from the tumor kinetics of (tracer) [^{11}C]docetaxel (data not shown), indicating that the present bevacizumab-induced decrease in [^{11}C]docetaxel uptake in tumors is likely to represent changes in tumor uptake of therapeutic doses of docetaxel.

The results of the present study pose a number of important issues relevant to anti-angiogenic drugs administered in combination with other anticancer drugs. In human tumors, bevacizumab induced a rapid decrease in perfusion and [^{11}C]docetaxel uptake. It is conceivable that other inhibitors of the VEGF signaling pathways may produce similar effects. In addition, it is likely that these effects may persist during continued treatment with these drugs. Therefore, administration of anti-angiogenic drugs can be considered after administration of the other anticancer agents, as the immediate decrease in tumor perfusion should decrease clearance of drugs from tumors. Hence, preclinical studies are warranted to investigate this concept for scheduling of anticancer drugs. To improve scheduling of combination therapy, other potential mechanisms need to be investigated to understand the synergistic effects with anti-angiogenic drugs. In this regard, it is important to explore the effects of anti-angiogenic drugs on proliferative activity of tumor cells (Ortholan et al., 2010) and their environment, such as mobilization of bone marrow-derived circulating endothelial progenitor cells (Shaked et al., 2008) and acute release of cytokines from the tumor microenvironment (Gilbert and Hemann, 2010).

The results of the present study may explain why several clinical trials have failed to show the additional value of anti-angiogenic drugs in specific populations of cancer patients. Clearly, more clinical studies are needed to assess whether administration schedules affect response and outcome of combination strategies. To this end, the optimal design to prove clinical relevance of drug scheduling would be a randomized controlled trial in which cancer patients are randomized to different administration schedules.

In conclusion, the results of this human study indicate a rapid and significant reduction in perfusion and [^{11}C]docetaxel uptake in NSCLC after administration of bevacizumab. The clinical relevance of these findings is notable, as the present study did not provide evidence for a substantial improvement in drug delivery to tumors but rather showed the opposite effect. These findings highlight the importance of drug scheduling and advocate further studies to optimize scheduling of anti-angiogenic drugs.

EXPERIMENTAL PROCEDURES

Patient Selection

Between October 2009 and September 2010, ten patients (six men and four women; median age 58 years; range, 47–70 years) with advanced-stage NSCLC were prospectively enrolled. Patients participated in this study prior to their scheduled therapy. The study was approved by the Medical Ethics Review Committee of the VU University Medical Center, Amsterdam. All patients signed a protocol-specific informed consent form prior to study enrollment.

Inclusion criteria were the following: age $\geq$18 years; a malignant lesion $\geq$1.5 cm in diameter within the chest; life expectancy of at least 12 weeks; Eastern Cooperative Oncology Group performance status <3; $\geq$4 weeks since any prior surgery or radiotherapy; no previous acute toxicities (>1) in accordance with Common Terminology Criteria for Adverse Events v3.0 (CTCAE); adequate organ function [hemoglobin $\geq$6.0 mmol·l^{-1}; absolute neutrophil count $\geq$1.5 × 10^9/l; absolute platelet count >100 × 10^9/l; total serum bilirubin $\leq$1.5 upper limit of normal (ULN); aspartate aminotransferase and alanine aminotransferase $\leq$2.5 x ULN (in case of liver metastases $\leq$ 5 x ULN); alkaline phosphatase $\leq$2.5 x ULN; serum creatinine $\leq$1.5 ULN or creatinine clearance $\geq$60 ml·min^{-1}; normal serum calcium; urine dipstick for proteinuria <2+]; and use of effective contraception.

Exclusion criteria were the following: squamous lung cancer; history of $\geq$ grade 2 hemoptysis; cavitary lesion; tumor invading major blood vessels; newly diagnosed and untreated central nervous system metastases; any unstable systemic disease (including but not limited to clinically significant cardiovascular disease and uncontrolled hypertension); major surgery or significant traumatic injury <28 days before study entry; prior treatment with taxanes or bevacizumab; concurrent treatment with other anticancer agents or experimental drugs; use of inhibitors or substrates of the efflux transporter ABCB1; serious nonhealing wound or ulcer; a history of documented hemorrhagic diathesis or coagulopathy; therapeutic anticoagulation; regular use of aspirin (>325 mg per day); planned radiotherapy or major surgery; pregnancy or lactation; metal implants (e.g., pacemakers); and claustrophobia.

Study Design

Patients received a single infusion of bevacizumab (15 mg·kg^{-1}, infused over 90 min). In the week prior to this infusion, patients underwent a dynamic PET-CT study with both [^{15}O]H_2O and [^{11}C]docetaxel. At 5 hr and 4 days after infusion of bevacizumab, the PET-CT protocol was repeated. In addition, 2 hr after infusion of bevacizumab, patients underwent an additional dynamic PET-CT scan with [^{15}O]H_2O. Sequential scans were possible because of the short half-lives of oxygen-15 and carbon-11, which are 2.0 and 20.3 min, respectively. Initially, the last time point for PET measurements was set at day 7. However, recruitment of patients seemed difficult, as patients were not willing

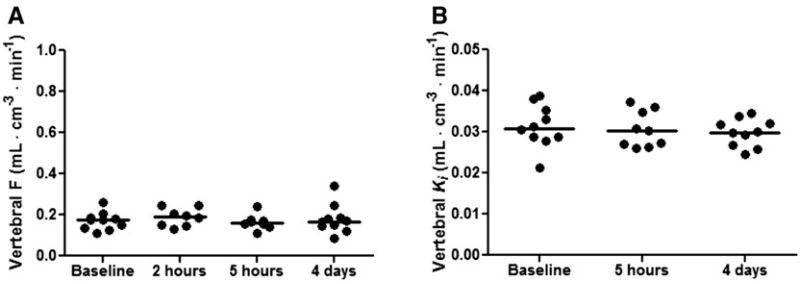

Figure 6. Perfusion and [^{11}C]docetaxel Uptake in the Vertebral Body, which Represents Bone Marrow, in Ten Individual Patients at Baseline and after Administration of Bevacizumab

Horizontal bars represent median values.

(A) Perfusion (F).

(B) Net rate of influx (K_i) of [^{11}C]docetaxel.

to postpone their planned chemotherapy for more than a few days. Hence, the protocol was amended and the last time point was set at day 4. Adverse events were graded in accordance with CTCAE v3.0. After the last PET-CT study, patients started with their scheduled therapy. In accordance with the guidelines of the Medical Ethics Review Committee of the VU University Medical Center, the total radiation burden of the study was estimated at <10 mSv. As efficacy was not an endpoint of the present study, response evaluation and data collection for survival were not performed.

Synthesis of Radiopharmaceuticals

The radiosyntheses of [^{15}O]H_2O and [^{11}C]docetaxel were performed in accordance with good manufacturing practice (GMP) standards (Jackson et al., 1993; van Tilburg et al., 2004 and 2008). Docetaxel, obtained from Green PlantChem Company (Hangzhou, China), was chemically modified and used as precursor in the synthesis of [^{11}C]docetaxel. ^{11}C-labeled docetaxel was obtained with an isolated decay-corrected radiochemical yield of 10 ± 2% and a radiochemical purity of >98%. [^{11}C]docetaxel has an identical molecular structure as the drug docetaxel. The identity of [^{11}C]docetaxel was confirmed by comparison of retention times on high-performance liquid chromatography with authentic docetaxel.

Scanning Protocol

Imaging studies were performed on a state-of-the-art three-dimensional (3D) PET-CT scanner (Gemini TF-64, Philips Medical Systems, Best, The Netherlands; Surti et al., 2007). This scanner has an axial field of view of 18 cm, divided into 45 contiguous planes. All patients underwent PET-CT scans with [^{15}O]H_2O and [^{11}C]docetaxel at baseline and at day 4. Nine patients underwent a [^{15}O]H_2O PET-CT scan at 2 hr and eight patients underwent combined [^{15}O]H_2O and [^{11}C]docetaxel PET-CT scans at 5 hr, whereas one patient underwent a single [^{11}C]docetaxel PET-CT scan at 5 hr. The median times from the end of the bevacizumab infusion to the first, second, and third scan sessions were 1.9 hr (range, 1.4–2.3 hr), 5.6 hr (range, 4.9–8.6 hr), and 4 days (range, 3–5 days). Sudden technical difficulties, clinical problems, and logistic issues were the reasons for missing scans and different time intervals.

Until 3 hr prior to scanning, food and drinks were allowed. On the day of a PET study, patients were asked to consume similar meals prior to scanning. All patients received two venous catheters, one for tracer injection and the other for blood sampling. Patients were positioned supine on the scanner bed, with both tumor and aortic arch located inside the axial field of view of the scanner. Elastic body-restraining bandages were used to minimize movement during scanning.

A 10 min dynamic scan was started simultaneously with an intravenous injection of 370 MBq [^{15}O]H_2O (5 ml at a rate of 0.8 ml·s^{-1}, followed by a 35 ml saline flush at a rate of 2 ml·s^{-1}). Thereafter, a 50 mAs low-dose CT scan was performed for attenuation correction purposes. At least 20 min after administration of [^{15}O]H_2O, a 60 min dynamic scan was started simultaneously with an intravenous injection of [^{11}C]docetaxel (dissolved in a maximum volume of 12 ml saline, infused at a rate of 0.8 ml·s^{-1}, and followed by a 35 ml saline flush at a rate of 2 ml·s^{-1}). The median injected dose of [^{11}C]docetaxel was 344 MBq (range, 122–388 MBq) with a median specific activity of 3.2 GBq·μmol^{-1} (range; 1.0–25.8 GBq·μmol^{-1}). During PET scanning, blood pressure was monitored with a Dinamap (Dash 4000, GE Medical Systems Information Technologies, Inc., Milwaukee, Wisconsin).

Data were normalized and all appropriate corrections for dead time, decay, randoms, scatter, and attenuation were applied. Using the 3D row action maximum likelihood reconstruction algorithm, [^{15}O]H_2O and [^{11}C]docetaxel scans were reconstructed into 26 (1x10, 8x5, 4x10, 2x15, 3x20, 2x30, and 6x60 s) and 36 (1x10, 8x5, 4x10, 2x15, 3x20, 2x30, 6x60, 4x150, 4x300, and 2x600 s) frames, respectively.

Blood Sampling

Sequential blood samples were collected in ACD vacutainers (8.5 ml, Becton Dickinson, Heidelberg, Germany; Cat. No. 364606) at baseline, and at 3 hr and 4 days after the end of the bevacizumab infusion. Prior to each sample, 3 ml–5 ml blood was discarded and the line was flushed with 2 ml saline after each sample. After collection, the blood samples were centrifuged immediately to obtain platelet-rich plasma (15 min; 20°C; 156 x *g*; N = 7 patients). Platelet-rich plasma was further centrifuged to obtain platelet-poor plasma (15 min; 20°C; 330 x *g*; N = 3 patients). Thereafter, plasma was stored at −20°C until analysis. Concentrations of VEGF (pg·ml^{-1}) were assessed in duplicate using a Quantikine enzyme-linked immunosorbent assay (ELISA) kit (R&D Systems, Minneapolis, Minnesota). Vascular endothelial growth factor concentrations in platelet-rich plasma were corrected for platelet count and were expressed in pg·ml^{-1} per 200,000 platelets·μl^{-1}.

After intravenous injection of [^{11}C]docetaxel, 10 ml discrete venous samples were collected manually at 2.5, 5, 10, 15, 20, 30, 40, and 60 min post-injection. Blood samples were analyzed for radioactivity concentrations in blood and plasma. Whole blood (0.5 ml) was weighted in duplicate and 0.05 ml 10% Triton X-100 solution was added. After centrifuging the remaining whole blood (5 min; room temperature; 4000 rpm), plasma was harvested and 0.5 ml plasma was weighted in duplicate, again adding 0.05 ml 10% Triton X-100 solution. A well-counter, cross-calibrated against the PET scanner, was used to determine activity concentrations. Samples were not analyzed for radiolabeled metabolites, as these were not detected previously (Van der Veldt et al., 2011).

Input Functions

Kinetic analyses of data were performed using dedicated programs written within the software environment Matlab (The MathWorks Inc., Natick, Massachusetts). The ascending aorta in the [^{15}O]H_2O and [^{11}C]docetaxel images was used to generate noninvasive image-derived input functions (IDIF), as validated previously (van der Veldt et al., 2010a and 2011). Volumes of interest (VOI) of 1 cm diameter were drawn over the ascending aorta in approximately ten consecutive image planes of the frame in which the first pass of the bolus was best visualized. Projection of these VOIs onto all image frames yielded the arterial time-activity curve (TAC) $C_A(t)$. A similar approach was used for the pulmonary artery in approximately five consecutive planes, thereby providing a TAC for the pulmonary circulation $C_V(t)$ (van der Veldt et al., 2010a). The [^{11}C]docetaxel plasma IDIF was obtained by multiplying $C_A(t)$ with a sigmoid function (Gunn et al., 1998), which was obtained by fitting the plasma/whole blood ratios derived from the venous samples. As the rapid [^{11}C]docetaxel clearance precludes reliable input functions at later time points, the generation of input functions of [^{11}C]docetaxel was limited to the first 10 min of data (Van der Veldt et al., 2011).

Analysis of Perfusion and [^{11}C]docetaxel Kinetics in Tumors

Scans were anonymized and randomly presented to an experienced observer (I.B.) who was blinded to patients' history and outcome. To delineate comparable tumor VOIs, this observer analyzed all scans from one patient in the same session. Low-dose CT images were converted to ECAT 7 format. Thereafter,

primary tumors were delineated on low-dose CT images using the CAPP software package (CTI/Siemens, Knoxville, Tennessee). Next, VOIs were projected onto the dynamic images of the corresponding $[^{15}O]H_2O$ and [^{11}C]docetaxel scans, thereby generating tumor TACs for $[^{15}O]H_2O$ and [^{11}C]docetaxel, respectively.

The standard single-tissue compartment model was used to derive tumor perfusion from $[^{15}O]H_2O$ kinetics (Hermansen et al., 1998; van der Veldt et al., 2010a). Using nonlinear regression, $[^{15}O]H_2O$ tumor TACs were fitted to the single-tissue compartment model using IDIF as arterial input function (van der Veldt et al., 2010a). The correction for pulmonary circulation blood volume was included, as it improves the quality of the fits without affecting tumor perfusion values. Using this approach, the absolute test-retest variability of tumor perfusion is 0.03 $ml \cdot cm^{-3} \cdot min^{-1}$ (van der Veldt et al., 2010a).

The kinetics of [^{11}C]docetaxel in tumors was described by a two-tissue irreversible compartment model, linearized using the Patlak method (Patlak et al., 1983). When applying the Patlak method to the first 10 min of dynamic PET data with the starting time at 2 min, the K_i of [^{11}C]docetaxel has an absolute test-retest variability of 0.003 $ml \cdot cm^{-3} \cdot min^{-1}$ (van der Veldt et al., 2011). In addition, the retention index of [^{11}C]docetaxel in tumor tissue was calculated by dividing the measured radioactivity concentration at 10 min post-injection by the integral of the plasma curve up to this time.

To analyze heterogeneity of tumor perfusion at the voxel level, parametric perfusion images were generated (van der Veldt et al., 2010a). Hence, IDIFs and a basis function implementation of the standard single-tissue compartment model were applied (Boellaard et al., 2005; Lodge et al., 2000; Watabe et al., 2005). Fifty logarithmically spaced, precomputed basis functions with F/V_T values, ranging from 0.1 to 2.0 min^{-1} were used and parametric perfusion images were postsmoothed with a Gaussian filter of 10 mm full width at half maximum. Then, VOIs previously defined on the low-dose CT scans were projected onto the parametric perfusion images. Next, voxel intensity histograms were generated for the whole VOI, its center and its rim. A voxel was considered to be part of the rim if at least one of the voxels in its 3D six-connected neighborhood was outside the defined VOI. In accordance with this method, the median baseline volume of the whole tumor VOI was 13.3 cm^3 (range, 1.7–278.5 cm^3) with center and rim accounting for median volumes of 2.5 cm^3 (range, 0.1–183.8 cm^3) and 9.1 cm^3 (range, 1.5–81.3 cm^3), respectively. Similarly, voxel intensity histograms were generated for the K_i of [^{11}C]docetaxel, applying the Patlak method on a voxel basis. The voxel intensity histograms were used to characterize tumor heterogeneity of perfusion and [^{11}C]docetaxel uptake, analyzing the following parameters: percentage of voxels, mean value, standard deviation, median value, minimal value, maximal value, kurtosis, and skewness of the distribution. More homogenous distributions are characterized by lower standard deviations and higher kurtosis (more peaked distribution) of corresponding histograms.

Cardiac Output

Using dynamic $[^{15}O]H_2O$ PET data, the cardiac output can be estimated by the following equation (Knaapen et al., 2008):

$$\text{Cardiac output} = \frac{\text{ID}}{\int_0^t C_V \cdot dt}, \quad (1)$$

where the injected radioactivity (ID) of $[^{15}O]H_2O$ is divided by the area under the curve of the blood activity in the pulmonary artery (C_V) multiplied by the duration of the first pass of the bolus. The TAC of the pulmonary artery was fitted with a linear upslope and followed by an exponential downslope, which was extrapolated to remove contamination of recirculating radioactivity.

Microcirculation in the Skin

In eight patients, microcirculation in the skin was investigated. At baseline, 3 hr and 4 days, nailfold capillaries in the dorsal skin of the third finger were visualized using a capillary microscope (Serné et al., 2001). Capillary density was defined as the number of erythrocyte-perfused capillaries $\cdot mm^{-2}$. First, baseline capillary density was recorded for 2 min. Thereafter, venous occlusion was applied to expose a maximal number of perfused capillaries. To this end, a digital cuff was inflated to 60 mmHg for 60 s. Recordings were presented randomly and in a blind fashion to an experienced investigator (M.P.d.B.), who counted number of capillaries off-line from a videotape. Using the same visual fields as used during baseline measurements, peak capillary density during venous congestion was counted in the 60 s recordings. Day-to-day variation of baseline capillary density and peak capillary density during venous congestion were 2.3% ± 1.8% (Serné et al., 2002) and 9.5 ± 7.1% (Serné et al., 2001), respectively.

Muscle Perfusion

On the low-dose CT scans, VOIs (diameter, 1 cm) were drawn over the erector spinae muscle in five consecutive image planes. Projection of these muscle VOIs onto the dynamic images of the corresponding $[^{15}O]H_2O$ scan yielded a muscle TAC for $[^{15}O]H_2O$. The standard single-tissue compartment model was used to derive muscle perfusion (Hermansen et al., 1998) but without correction for pulmonary circulation blood volume:

$$C_T(t) = (1 - V_A) \cdot F \cdot C_A(t) \otimes e^{-\frac{F}{V_T} t} + V_A \, C_A(t), \quad (2)$$

where $C_T(t)$ is the total measured tissue signal in tumor as function of time, F is perfusion, V_A is arterial blood volume, and V_T is the volume of distribution or partition coefficient of water. To evaluate [^{11}C]docetaxel kinetics in normal tissue, muscle VOIs were also projected onto the corresponding [^{11}C]docetaxel image and those TACs were analyzed using the Patlak method (Patlak et al., 1983).

[^{11}C]docetaxel Clearance

To determine influence of bevacizumab on blood kinetics of [^{11}C]docetaxel, clearance of [^{11}C]docetaxel was calculated using the following equation:

$$\text{Clearance} = \frac{\text{ID}}{\int C_P(t) \cdot dt \cdot \text{BSA}}, \quad (3)$$

where the injected dose (ID) of [^{11}C]docetaxel is divided by the integral of the plasma (C_P) TAC multiplied by the body surface area.

Thyroid Perfusion

In those cases in which the thyroid gland was in the field of view, additional parametric perfusion images were generated, using 50 precomputed basis functions with F/V_T values, ranging from 0.1 to 15 min^{-1} and postsmoothing with a Gaussian filter of 10 mm in full width at half maximum. Then, the thyroid gland could be delineated on parametric perfusion images applying a semi-automatic threshold technique (50% of the maximum voxel value with correction for local background; van der Veldt et al., 2010a). Thereafter, these VOIs were projected onto the dynamic $[^{15}O]H_2O$ images. Again, the standard single-tissue compartment model (Equation 2) was applied to calculate perfusion.

Perfusion and [^{11}C]docetaxel Kinetics in Bone Marrow

Perfusion and [^{11}C]docetaxel uptake were determined in the vertebral body, representing active bone marrow. From the level of the main carina to ten image planes downwards, VOIs (diameter, 1.5 cm) were defined in the vertebral body on low-dose CT scans. These VOIs were projected onto dynamic images of the $[^{15}O]H_2O$ and [^{11}C]docetaxel scans, generating corresponding TACs.

Equation 2 was applied to calculate vertebral body perfusion, whereas the Patlak method (Patlak et al., 1983) was applied to determine [^{11}C]docetaxel uptake.

Statistics

Statistical analysis was performed using SPSS software (SPSS for Windows 16.0, SPSS, Inc., Chicago, IL). Correlations were explored using the Spearman's correlation coefficient. The Mann-Whitney test was used to compare between groups. The Wilcoxon signed-rank test was used to compare variables at 2 hr, 3 hr, 5 hr, and 4 days after bevacizumab administration with baseline values. A two-tailed probability value of p value < 0.05 was considered significant.

ACKNOWLEDGMENTS

The authors would like to thank all patients who participated in this study. In addition, the authors would like to thank Suzette van Balen, Amina

Elouahmani, Judith van Es, Robin Hemminga, Femke Jongsma, Nghi Pham, Nasserah Sais, and Jeroen Wilhelmus for scanning the patients, Emile Comans, Otto Hoekstra, Daniela Oprea-Lager, Pieter Raijmakers, Nafees Rizvi, Natasja Kok, Ilona Pomstra, Atie van Wijk, Sabri Duzenli, Martijn Groenendijk, Esther Nossent, Arifa Pašić, Suzy Samii, Serge van Wolferen, and Jennifer Benit for help with logistical planning and patient care, Ronald Boellaard, Dennis Boersma, Marc Huisman, Arthur van Lingen, and Maqsood Yaqub for technical assistance; Peter van de Ven for statistical advice; Bart Kuenen for help with the design of the study; Martien Mooijer, Anneloes Rijnders, and Dennis Laan for production of [^{11}C]docetaxel; Henk Dekker for help with the analyses of VEGF levels; and Marissa Rongen, Robert Schuit, and Kevin Takkenkamp for the production of [^{15}O]H_2O and the analysis of blood samples. This work was supported by a grant of the Cancer Center Amsterdam. This study was presented in part at the 2011 ASCO Annual Meeting, Chicago, IL, June 3–7, 2011, #3059; and at the 14th World Conference on Lung Cancer, Amsterdam, The Netherlands, July 3–7, 2011, #O18.02.

Received: July 23, 2011
Revised: November 2, 2011
Accepted: November 29, 2011
Published: January 17, 2012

REFERENCES

Batchelor, T.T., Sorensen, A.G., di Tomaso, E., Zhang, W.T., Duda, D.G., Cohen, K.S., Kozak, K.R., Cahill, D.P., Chen, P.J., Zhu, M., et al. (2007). AZD2171, a pan-VEGF receptor tyrosine kinase inhibitor, normalizes tumor vasculature and alleviates edema in glioblastoma patients. Cancer Cell *11*, 83–95.

Boellaard, R., Knaapen, P., Rijbroek, A., Luurtsema, G.J., and Lammertsma, A.A. (2005). Evaluation of basis function and linear least squares methods for generating parametric blood flow images using 15O-water and Positron Emission Tomography. Mol. Imaging Biol. *7*, 273–285.

Carmeliet, P. (2000). Mechanisms of angiogenesis and arteriogenesis. Nat. Med. *6*, 389–395.

Chen, H.X., and Cleck, J.N. (2009). Adverse effects of anticancer agents that target the VEGF pathway. Nat. Rev. Clin. Oncol. *6*, 465–477.

Cobleigh, M.A., Langmuir, V.K., Sledge, G.W., Miller, K.D., Haney, L., Novotny, W.F., Reimann, J.D., and Vassel, A. (2003). A phase I/II dose-escalation trial of bevacizumab in previously treated metastatic breast cancer. Semin. Oncol. *30* (*Suppl 16*), 117–124.

Curti, B.D., Urba, W.J., Alvord, W.G., Janik, J.E., Smith, J.W., 2nd, Madara, K., and Longo, D.L. (1993). Interstitial pressure of subcutaneous nodules in melanoma and lymphoma patients: changes during treatment. Cancer Res. (*Suppl*). *53*, 2204–2207.

Dhaun, N., and Webb, D.J. (2010). Receptor tyrosine kinase inhibition, hypertension, and proteinuria: is endothelin the smoking gun? Hypertension *56*, 575–577.

Dunnwald, L.K., Gralow, J.R., Ellis, G.K., Livingston, R.B., Linden, H.M., Specht, J.M., Doot, R.K., Lawton, T.J., Barlow, W.E., Kurland, B.F., et al. (2008). Tumor metabolism and blood flow changes by positron emission tomography: relation to survival in patients treated with neoadjuvant chemotherapy for locally advanced breast cancer. J. Clin. Oncol. *26*, 4449–4457.

Ferrara, N., and Kerbel, R.S. (2005). Angiogenesis as a therapeutic target. Nature *438*, 967–974.

Ferrara, N., Gerber, H.P., and LeCouter, J. (2003). The biology of VEGF and its receptors. Nat. Med. *9*, 669–676.

Ferrara, N., Hillan, K.J., Gerber, H.P., and Novotny, W. (2004). Discovery and development of bevacizumab, an anti-VEGF antibody for treating cancer. Nat. Rev. Drug Discov. *3*, 391–400.

Gambhir, S.S. (2002). Molecular imaging of cancer with positron emission tomography. Nat. Rev. Cancer *2*, 683–693.

Gilbert, L.A., and Hemann, M.T. (2010). DNA damage-mediated induction of a chemoresistant niche. Cell *143*, 355–366.

Griffon-Etienne, G.E., Boucher, Y., Brekken, C., Suit, H.D., and Jain, R.K. (1999). Taxane-induced apoptosis decompresses blood vessels and lowers interstitial fluid pressure in solid tumors: clinical implications. Cancer Res. *59*, 3776–3782.

Gunn, R.N., Sargent, P.A., Bench, C.J., Rabiner, E.A., Osman, S., Pike, V.W., Hume, S.P., Grasby, P.M., and Lammertsma, A.A. (1998). Tracer kinetic modeling of the 5-HT1A receptor ligand [carbonyl-11C]WAY-100635 for PET. Neuroimage *8*, 426–440.

Hanahan, D., and Weinberg, R.A. (2000). The hallmarks of cancer. Cell *100*, 57–70.

Hermansen, F., Rosen, S.D., Fath-Ordoubadi, F., Kooner, J.S., Clark, J.C., Camici, P.G., and Lammertsma, A.A. (1998). Measurement of myocardial blood flow with oxygen-15 labelled water: comparison of different administration protocols. Eur. J. Nucl. Med. *25*, 751–759.

Hoekstra, C.J., Stroobants, S.G., Hoekstra, O.S., Smit, E.F., Vansteenkiste, J.F., and Lammertsma, A.A. (2002). Measurement of perfusion in stage IIIA-N2 non-small cell lung cancer using H(2)(15)O and positron emission tomography. Clin. Cancer Res. *8*, 2109–2115.

Hurwitz, H., Fehrenbacher, L., Novotny, W., Cartwright, T., Hainsworth, J., Heim, W., Berlin, J., Baron, A., Griffing, S., Holmgren, E., et al. (2004). Bevacizumab plus irinotecan, fluorouracil, and leucovorin for metastatic colorectal cancer. N. Engl. J. Med. *350*, 2335–2342.

Jackson, J.R., Dembowski, B.S., Ehrenkaufer, R.L., McIntyre, E., and Reivich, M. (1993). [15O]H2O, [15O]O2 and [15O]CO gas production, monitoring and quality control system. Appl. Radiat. Isot. *44*, 631–634.

Jain, R.K. (2001). Normalizing tumor vasculature with anti-angiogenic therapy: a new paradigm for combination therapy. Nat. Med. *7*, 987–989.

Jain, R.K. (2005). Normalization of tumor vasculature: an emerging concept in antiangiogenic therapy. Science *307*, 58–62.

Kamba, T., Tam, B.Y., Hashizume, H., Haskell, A., Sennino, B., Mancuso, M.R., Norberg, S.M., O'Brien, S.M., Davis, R.B., Gowen, L.C., et al. (2006). VEGF-dependent plasticity of fenestrated capillaries in the normal adult microvasculature. Am. J. Physiol. Heart Circ. Physiol. *290*, H560–H576.

Knaapen, P., Lubberink, M., Rijzewijk, L.J., van der Meer, R.W., Unger, M., Germans, T., Bax, J.J., Smit, J.W., Lamb, H.J., van Rossum, A.C., et al. (2008). Stroke volume measurements with first-pass dynamic positron emission tomography: comparison with cardiovascular magnetic resonance. J. Nucl. Cardiol. *15*, 218–224.

Kudoh, S., Takeda, K., Nakagawa, K., Takada, M., Katakami, N., Matsui, K., Shinkai, T., Sawa, T., Goto, I., Semba, H., et al. (2006). Phase III study of docetaxel compared with vinorelbine in elderly patients with advanced non-small-cell lung cancer: results of the West Japan Thoracic Oncology Group Trial (WJTOG 9904). J. Clin. Oncol. *24*, 3657–3663.

Lodge, M.A., Carson, R.E., Carrasquillo, J.A., Whatley, M., Libutti, S.K., and Bacharach, S.L. (2000). Parametric images of blood flow in oncology PET studies using [15O]water. J. Nucl. Med. *41*, 1784–1792.

Miller, K., Wang, M., Gralow, J., Dickler, M., Cobleigh, M., Perez, E.A., Shenkier, T., Cella, D., and Davidson, N.E. (2007). Paclitaxel plus bevacizumab versus paclitaxel alone for metastatic breast cancer. N. Engl. J. Med. *357*, 2666–2676.

Mourad, J.J., des Guetz, G., Debbabi, H., and Levy, B.I. (2008). Blood pressure rise following angiogenesis inhibition by bevacizumab. A crucial role for microcirculation. Ann. Oncol. *19*, 927–934.

Ng, Q.S., Goh, V., Milner, J., Stratford, M.R., Folkes, L.K., Tozer, G.M., Saunders, M.I., and Hoskin, P.J. (2007). Effect of nitric-oxide synthesis on tumour blood volume and vascular activity: a phase I study. Lancet Oncol. *8*, 111–118.

Ortholan, C., Durivault, J., Hannoun-Levi, J.M., Guyot, M., Bourcier, C., Ambrosetti, D., Safe, S., and Pagès, G. (2010). Bevacizumab/docetaxel association is more efficient than docetaxel alone in reducing breast and prostate cancer cell growth: a new paradigm for understanding the therapeutic effect of combined treatment. Eur. J. Cancer *46*, 3022–3036.

Patlak, C.S., Blasberg, R.G., and Fenstermacher, J.D. (1983). Graphical evaluation of blood-to-brain transfer constants from multiple-time uptake data. J. Cereb. Blood Flow Metab. *3*, 1–7.

Reese, D., Fratesi, P., Corry, M., Novotny, W., Holmgren, E., and Small, E. (2001). A phase II trial of humanized anti-vascular endothelial growth factor antibody for the treatment of androgen-independent prostate cancer. The Prostate J. *3*, 65–70.

Sandler, A., Gray, R., Perry, M.C., Brahmer, J., Schiller, J.H., Dowlati, A., Lilenbaum, R., and Johnson, D.H. (2006). Paclitaxel-carboplatin alone or with bevacizumab for non-small-cell lung cancer. N. Engl. J. Med. *355*, 2542–2550.

Serné, E.H., Gans, R.O., ter Maaten, J.C., Tangelder, G.J., Donker, A.J., and Stehouwer, C.D. (2001). Impaired skin capillary recruitment in essential hypertension is caused by both functional and structural capillary rarefaction. Hypertension *38*, 238–242.

Serné, E.H., IJzerman, R.G., Gans, R.O., Nijveldt, R., De Vries, G., Evertz, R., Donker, A.J., and Stehouwer, C.D. (2002). Direct evidence for insulin-induced capillary recruitment in skin of healthy subjects during physiological hyperinsulinemia. Diabetes *51*, 1515–1522.

Shaked, Y., Henke, E., Roodhart, J.M., Mancuso, P., Langenberg, M.H., Colleoni, M., Daenen, L.G., Man, S., Xu, P., Emmenegger, U., et al. (2008). Rapid chemotherapy-induced acute endothelial progenitor cell mobilization: implications for antiangiogenic drugs as chemosensitizing agents. Cancer Cell *14*, 263–273.

Shalli, K., Brown, I., Heys, S.D., and Schofield, A.C. (2005). Alterations of beta-tubulin isotypes in breast cancer cells resistant to docetaxel. FASEB J. *19*, 1299–1301.

Surti, S., Kuhn, A., Werner, M.E., Perkins, A.E., Kolthammer, J., and Karp, J.S. (2007). Performance of Philips Gemini TF PET/CT scanner with special consideration for its time-of-flight imaging capabilities. J. Nucl. Med. *48*, 471–480.

Syrigos, K.N., Karapanagiotou, E., Boura, P., Manegold, C., and Harrington, K. (2011). Bevacizumab-induced hypertension: pathogenesis and management. BioDrugs *25*, 159–169.

van der Veldt, A.A., Hendrikse, N.H., Harms, H.J., Comans, E.F., Postmus, P.E., Smit, E.F., Lammertsma, A.A., and Lubberink, M. (2010a). Quantitative parametric perfusion images using 15O-labeled water and a clinical PET/CT scanner: test-retest variability in lung cancer. J. Nucl. Med. *51*, 1684–1690.

Van der Veldt, A.A., Hendrikse, N.H., Smit, E.F., Mooijer, M.P., Rijnders, A.Y., Gerritsen, W.R., van der Hoeven, J.J., Windhorst, A.D., Lammertsma, A.A., and Lubberink, M. (2010b). Biodistribution and radiation dosimetry of 11C-labelled docetaxel in cancer patients. Eur. J. Nucl. Med. Mol. Imaging *37*, 1950–1958.

Van der Veldt, A.A., Lubberink, M., Greuter, H.N., Comans, E.F., Herder, G.J., Yaqub, M., Schuit, R.C., Van Lingen, A., Rizvi, S.N., Mooijer, M.P., et al. (2011). Absolute quantification of [11C]docetaxel kinetics in lung cancer patients using positron emission tomography. Clin. Cancer Res. *15*, 4814–4824.

van Tilburg, E.W., Franssen, E.J., Van der Hoeven, J.J., Van der Meij, M., Elshove, D., Lammertsma, A.A., and Windhorst, A.D. (2004). Radiosynthesis of [11C]docetaxel. J. Labelled Comp. Rad. *47*, 763–777.

van Tilburg, E.W., Mooijer, M.P., Brinkhorst, J., van der Meij, M., and Windhorst, A.D. (2008). Improved and semi-automated GMP-compliant radiosynthesis of [11C]docetaxel. Appl. Radiat. Isot. *66*, 1414–1418.

Verheul, H.M., Hoekman, K., Luykx-de Bakker, S., Eekman, C.A., Folman, C.C., Broxterman, H.J., and Pinedo, H.M. (1997). Platelet: transporter of vascular endothelial growth factor. Clin. Cancer Res. *3*, 2187–2190.

Watabe, H., Jino, H., Kawachi, N., Teramoto, N., Hayashi, T., Ohta, Y., and Iida, H. (2005). Parametric imaging of myocardial blood flow with 15O-water and PET using the basis function method. J. Nucl. Med. *46*, 1219–1224.

Willett, C.G., Boucher, Y., di Tomaso, E., Duda, D.G., Munn, L.L., Tong, R.T., Chung, D.C., Sahani, D.V., Kalva, S.P., Kozin, S.V., et al. (2004). Direct evidence that the VEGF-specific antibody bevacizumab has antivascular effects in human rectal cancer. Nat. Med. *10*, 145–147.

Wilson, C.B., Lammertsma, A.A., McKenzie, C.G., Sikora, K., and Jones, T. (1992). Measurements of blood flow and exchanging water space in breast tumors using positron emission tomography: a rapid and noninvasive dynamic method. Cancer Res. *52*, 1592–1597.

Yang, J.C., Haworth, L., Sherry, R.M., Hwu, P., Schwartzentruber, D.J., Topalian, S.L., Steinberg, S.M., Chen, H.X., and Rosenberg, S.A. (2003). A randomized trial of bevacizumab, an anti-vascular endothelial growth factor antibody, for metastatic renal cancer. N. Engl. J. Med. *349*, 427–434.